

Scalable MCMC for Bayes Shrinkage Priors

James E. Johndrow*
 Stanford University, Stanford, CA USA
 johndrow@stanford.edu

Paulo Orenstein*
 Stanford University, Stanford, CA USA
 pauloo@stanford.edu

December 7, 2021

Abstract

Gaussian scale mixture priors are frequently employed in Bayesian analysis of high-dimensional models, and a theoretical literature exists showing optimal risk properties of several members of this family in $p \gg n$ settings when the truth is sparse. However, while implementations of frequentist methods such as the Lasso can scale to dimension in the hundreds of thousands, corresponding Bayesian methods that use MCMC for computation are often limited to problems at least an order of magnitude smaller. This is in large part due to convergence toward unity of the spectral gap of the associated Markov kernel as the dimension grows. Here we propose an MCMC algorithm for computation in these models that combines blocked Gibbs, Metropolis-Hastings, and slice sampling. Our algorithm has computational cost per step comparable to the best existing alternatives, but superior convergence properties, giving effective sample sizes of 50 to 100 fold larger for identical computation time. Moreover, the convergence rate of our algorithm deteriorates much more slowly than alternatives as the dimension grows. We illustrate the scalability of the algorithm in simulations with up to 20,000 predictors.

Keywords: computational complexity; global-local; Markov chain Monte Carlo; scalability.

1 Introduction

Consider a generalized linear model with likelihood

$$y_i \stackrel{iid}{\sim} L(y_i \mid x_i \beta), \quad i = 1, \dots, n, \quad (1)$$

where β is assumed to be a sparse vector. A common hierarchical Bayesian approach when $p \gg n$ is to use a Gaussian scale-mixture prior on parameters of the form

$$\beta_j \stackrel{iid}{\sim} N(0, \tau^2 \lambda_j^2), \quad \tau \sim \pi_\tau(\cdot), \quad \lambda_j \sim \pi_\lambda(\cdot), \quad j = 1, \dots, p.$$

For appropriate choice of π_λ , this prior structure induces approximate sparsity in β by shrinking most components aggressively toward zero while retaining the true signals [14]. In this sense, the prior approximates the properties of point-mass mixture priors [19, 5], which allow some components of β to be exactly zero *a posteriori*. From the point of view of testing $H_{0j} : \beta_j = 0$, the global scale parameter τ controls how many of the hypotheses are true, while the local scales λ_j control which of the hypotheses are true, resulting in the designation “global-local” for this prior structure [14].

Here we focus on the case where (1) is the Gaussian linear model, although various data augmentation strategies allow our algorithm to easily extend to most generalized linear models.

*Authors are listed alphabetically.

For the Gaussian linear model, we have $f(y_i | x_i \beta) = (2\pi\sigma^2)^{-1/2} \exp\{-(y_i - x_i \beta)^2/(2\sigma^2)\}$, and it is common to scale the prior on β by the residual variance, giving $\beta_j \sim N(0, \sigma^2 \tau^2 \lambda_j^2)$.

Numerous choices of π_λ specially designed for high dimensions have been proposed. These include the Bayes Lasso induced by the Laplace prior $\pi_\lambda(z) \propto z \exp(-z^2/2)$ [13, 22], the generalized double Pareto $\pi_\lambda(z) \propto (2\xi)^{-1} (1 + |z|(\alpha\xi)^{-1})^{-(\alpha+1)}$ [1], and the Strawderman-Berger prior $\pi_\lambda(z) \propto z(1 + z^2)^{-3/2}$ [21]. Arguably, the most popular of these is the Horseshoe prior, which uses independent standard Cauchy priors $\pi_\lambda(z) \propto (1 + z^2)^{-1}$. Recent results show that, like point-mass mixtures, some priors of this class achieve the minimax-optimal rate of posterior convergence in high-dimensional settings. This includes the Horseshoe [23], as well as the Dirichlet-Laplace prior of Bhattacharya et al. [3].

In this paper we focus on the horseshoe, but generalizations to other global-local priors are straightforward. Our model setup is as follows:

$$\begin{aligned} y_i | \beta_j, \lambda_j, \tau &\stackrel{iid}{\sim} N(x_i \beta, \sigma^2) \\ \beta_j &\stackrel{iid}{\sim} N(0, \tau^2 \lambda_j^2) \\ \lambda_j &\stackrel{iid}{\sim} \frac{1}{1 + \lambda_j^2} \\ \tau &\sim \frac{1}{1 + \tau^2} \\ \sigma^2 &\sim \text{InvGamma}(a_0/2, b_0/2), \end{aligned}$$

where the observations range from $i = 1, \dots, n$ and the predictors $j = 1, \dots, p$.

Ostensibly, a major advantage of local-global priors relative to point-mass mixtures is the reduced computational complexity and the ability to handle larger problem sizes. Computation in these models is almost always performed by MCMC. The computational complexity of MCMC is a function of (i) the computational complexity of taking one step from the associated transition kernel P (“cost per step”); and (ii) the rate at which the Markov path length necessary to achieve any fixed Monte Carlo error goes to zero in n and p (the “spectral gap effect”). We use “spectral gap effect” as an informal designation for the second factor, since in most cases of interest, the computational complexity of MCMC is approximately the sum of the cost per step and the rate at which the spectral gap converges to zero as $n, p \rightarrow \infty$. Analysis of cost per step is a relatively straightforward exercise in classical computational complexity analysis. N雖ive algorithms for propagating P for models with global-local priors are $\mathcal{O}(p^3)$ per step because of the need to solve a linear system, but a significant improvement in the $p \gg n$ case — to $\mathcal{O}(n^2 p)$ — can be achieved using the Gaussian sampling algorithm of Bhattacharya et al. [2].

Analysis of the rate at which the spectral gap converges to zero is more complicated, and it depends on properties of the Markov kernel. This component of computational complexity can also be understood in terms of the autocorrelation structure of the Markov chain — represented, for example, via the integrated autocorrelation time — and the rate at which the integrated autocorrelation time converges to infinity with n and p . In cases where P is reversible, the integrated autocorrelation time is bounded by the inverse of the $L^2(\mu)$ spectral gap, where μ is the posterior measure. The details of these relationships are outlined in Section 3. Since the cost per step of MCMC is generally similar to, or worse than, the per iteration complexity of comparable optimization algorithms, an MCMC algorithm that scales to similar problem size must have a spectral gap that is nearly independent of, or decreasing in, n and p .

Existing theoretical analysis of MCMC algorithms for posterior computation with global-local priors consists of showing a geometric ergodicity result with n, p fixed [9, 12, 17]. In Khare and Hobert [9] and Pal and Khare [12], the authors consider the Gibbs sampling algorithm of Park and Casella [13] and Bhattacharya et al. [3] for the Bayes Lasso and Dirichlet-Laplace priors, respectively. Rajaratnam et al. [17] consider a blocked Gibbs sampler for Bayes Lasso obtained by sampling σ^2 marginal of β ; Polson et al. [15, Supplement §A.2] also use this update in the normal means setting. Also in [17], the authors note that their bound on the geometric convergence rate tends to 1 at an exponential rate in n, p , which would indicate the algorithm is NP-hard via the effect on the spectral gap. This is inconsistent with empirical performance, so the bound appears to be loose. In general, bounds on the geometric convergence rate and spectral gap obtained

from the sort of Foster-Lyapunov/small set arguments in [9, 12, 17] can be loose to the point of being uninformative about the actual performance of the algorithm, even in very simple cases (see Diaconis et al. [4] for numerous examples of cases where the mixing times obtained using drift and minorization arguments are provably many orders of magnitude worse than the true mixing times). Moreover, they generally provide little information about how the algorithm scales in n, p , as the bounds usually go to 1 at an exponential rate in n, p [16]. It seems likely that this reflects the inherent difficulty of finding “good” Lyapunov functions for specific kernels rather than any fundamental deficiencies of the theory.

Thorough empirical analysis of algorithms for Bayes Lasso [7] and Horseshoe [15, Supplement] priors have been undertaken. It is clear from these studies that the major factor contributing to slow mixing is high autocorrelation for the global scale parameter τ , and that in general, mixing deteriorates as p increases. Hans [7] proposes two alternatives to the sampler of Park and Casella [13] which improve mixing, but come at an increased computational cost per step. Polson et al. [15] consider both slice sampling and parameter expansion for sampling τ , and find that parameter expansion offers only modest gains. Makalic and Schmidt [11] proposes a Gibbs sampler for the Horseshoe, though empirical comparison is only made to the slow implementation in the R package `monomvn`, rather than to the considerably faster algorithms of Polson et al. [15], or the current state of the art algorithm of Bhattacharya et al. [2].

To our knowledge, all existing MCMC algorithms for global-local priors consist of the following components: (1) Gibbs updates for β and σ^2 , or a block Gibbs update for β, σ^2 ; (2) Slice sampling, Gibbs, or parameter-expanded Gibbs updates for τ ; (3) Slice sampling, Gibbs, or parameter-expanded Gibbs updates for λ ; and/or (4) A block Gibbs update for τ, λ (only for the Dirichlet-Laplace prior of Bhattacharya et al. [3]). In Polson et al. [15], the authors conjecture that “an algorithm that will solve the problem of autocorrelation in τ must marginalize over the λ_j ’s” in either the update for τ or the update for β . In fact, the sampler of Bhattacharya et al. [3] does this for the Dirichlet-Laplace prior, and empirically results in better mixing. However, their Gibbs update is not generalizable to other local-global priors. Here, we take a different approach, and design a sampler with the following update rule:

1. Sample $\beta, \sigma^2, \tau \mid \lambda$ in a block by sampling $\tau \mid \lambda$, then $\sigma^2 \mid \tau, \lambda$, and finally $\beta \mid \sigma^2, \tau, \lambda$; and
2. Sample $\lambda \mid \beta, \sigma^2, \tau$ using slice sampling.

Block updates have long been recognized as a useful strategy for improving mixing and convergence properties (e.g. [20, pg. 5]). Moreover, the slow mixing for τ observed by Polson et al. [15] could also be explained by high dependence between τ, λ , and β , rather than just τ and λ , suggesting an intuitive explanation for why our algorithm should improve mixing. Although we focus on the Horseshoe prior, our algorithm is applicable to any global-local prior, so long as the λ_j are *a priori* independent. This includes every example we are aware of, except the Dirichlet-Laplace.

The first step of our block update is a Metropolis-Hastings step using a random walk proposal on $\log(\xi)$, where $\tau^{-2} = \xi$ is the global precision. This is the critical component; the posterior for ξ is heavy-tailed, and we provide intuition for why the random walk on the logarithm behaves in the right way under these circumstances. We show that for the particular case of the Horseshoe, our sampler is superior to existing alternatives, achieving orders of magnitude better effective sample sizes with nearly identical computation time per step. We empirically estimate the reciprocal effective sample size T_e^{-1} , which is approximately proportional to the spectral gap, as a function of p and n . We show that for our algorithm $T_e^{-1} \propto p^{0.24}$, compared to $T_e^{-1} \propto p^{0.91}$ for the algorithm of Bhattacharya et al. [2], and that T_e^{-1} actually decreases as a function of n for the range of problem sizes we consider. The practical scalability of our algorithm is further demonstrated by obtaining Markov paths of length 40,000 for $p = 20,000, n = 1000$ on a standard desktop computer in computation time of about five hours. Our code is available on GitHub.¹

¹https://github.com/jamesjohndrow/horseshoe_jo

2 The MCMC algorithm

Before giving details of the algorithm, we define a reparametrization to the precision scale, letting

$$\xi = \tau^{-2}, \quad \eta_j = \lambda_j^{-2}.$$

The slice sampler of Polson et al. [15], which is a component of our update, operates on this scale, as does our Metropolis-Hastings update for ξ .

Our sampler has the update rule

1. Propose $\log(\xi^*) \sim N(\log(\xi), s)$, then compute the log acceptance ratio

$$\log(q) = \log \left(\frac{L(y | \xi^*, \eta)}{L(y | \xi, \eta)} \frac{\pi_\xi(\xi^*)}{\pi_\xi(\xi)} \frac{\xi^*}{\xi} \right),$$

where the log-likelihood is given by

$$\log\{L(y | \xi, \eta)\} = -\frac{1}{2} \log|M| - \frac{(n + a_0)}{2} \log(b_0/2 + y^T M^{-1} y/2),$$

with $|M|$ denoting the determinant of the matrix

$$M = I_n + \xi^{-1} X \text{diag}(\eta^{-1}) X^T, \quad (2)$$

and the change of measure factor

$$\pi_\xi(\xi) = \frac{1}{\sqrt{\xi}(1 + \xi)}.$$

Then accept ξ^* with probability $\min\{q, 1\}$. We find that taking $s = 0.8$ results in good performance for all values of n, p we consider.

2. Sample $\sigma^2 | \eta, \xi$ from

$$\sigma^2 | \eta, \xi \sim \text{InvGamma} \left(\frac{a_0 + n}{2}, \frac{y^T M^{-1} y + b_0}{2} \right)$$

where M is defined as in (2).

3. Sample

$$\beta | \sigma^2, \xi, \eta \sim N((X^T X + \text{diag}(\eta \xi))^{-1} X^T y, \sigma^2 (X^T X + \text{diag}(\eta \xi))^{-1})$$

using the algorithm of Bhattacharya et al. [2].

4. Update η_j from independent conditionals using slice sampling. Specifically, sample

$$u \sim \text{Unif} \left(0, \frac{1}{\eta + 1} \right),$$

then sample η_j from an exponential distribution with rate

$$m = \frac{\beta_j^2 \xi}{2\sigma^2}$$

truncated to the interval $(0, r)$, where $r = \frac{1-u}{u}$. This is done by sampling $v \sim \text{Unif}(0, 1)$ and setting

$$\eta_j = -\frac{\log[1 - \{1 - \exp(-mr)\}v]}{m}. \quad (3)$$

Detailed calculations to derive this update rule are given in the Appendix.

These steps define a block update for $\xi, \sigma^2, \beta \mid \eta$ and a simple update for $\eta \mid \xi, \sigma^2, \beta$. This is in contrast to the algorithms of Polson et al. [15] and Rajaratnam et al. [17], which only block update β, σ^2 . Since the slow mixing parameter is ξ , block updating β, σ^2 is not expected to be as effective as a block update that includes ξ . Our algorithm shares the slice sampling update for η with the algorithms of Polson et al. [15] and Bhattacharya et al. [2], but our use of (3) appears to be more numerically stable than the algorithms of Polson et al. [15] and Bhattacharya et al. [2].² In fact, Bhattacharya et al. [2] relies on several truncations steps, which replace τ^2, λ_j^2 , or σ^2 with a fixed numeric value (between 10^{-8} and 10^{-10}) if the sampled value is smaller than the specified threshold. In the Appendix, we show that these truncations actually prevent the algorithm from converging in some cases. In contrast, our algorithm uses only a single truncation rule: we replace η_j with machine ϵ if η_j underflows.³ We detect no evidence of non-convergence using this rule, and in all of the simulations reported here, it was not invoked. All comparisons that follow between our algorithm and that of Bhattacharya et al. [2] therefore use (3) in place of the higher-level function calls in Bhattacharya et al. [2], and remove the truncation rules of Bhattacharya et al. [2], replacing them with our single truncation rule.

3 Measures of performance

We use several measures of performance to compare algorithms. The first are estimates of lag- k autocorrelations at stationarity,

$$\rho_k = \text{Cor}(X_k, X_0),$$

where $X_0 \sim \mu$. Estimates of ρ_k are obtained using the `coda` package for R after discarding a burn-in period of 1,000 iterations, and are denoted $\widehat{\rho}_k$.

The second measure of performance is the *effective sample size*, which is related to the asymptotic variance of the Markov chain. Suppose P is the transition kernel of a geometrically ergodic Markov chain, i.e. there exists a μ -measurable function $V : \mathcal{X} \rightarrow [1, \infty)$, where \mathcal{X} is the state space, and constants $\gamma \in (0, 1)$, $C < \infty$ for which

$$\|P^k(x_0, \cdot) - \mu\|_V \leq C\gamma^k V(x_0)$$

where

$$\|\mu - \nu\|_V = \sup_{|\varphi| \leq V} \int_{\mathcal{X}} \varphi(x)(\mu - \nu)(dx).$$

is a *weighted* total variation norm. For any μ -measurable $f^2 < V$, let $\rho_k(f) = \text{Cor}(f(X_0), f(X_k))$ and define the asymptotic variance as

$$\sigma_f^2 = \text{Var}_{\mu}(f) \left[1 + 2 \sum_{k=1}^{\infty} \rho_k(f) \right]. \quad (4)$$

The quantity inside the brackets in (4) is called the integrated autocorrelation time. Then, since $f^2 < V$, $0 \leq \sigma_f^2 < \infty$, and, if $\sigma_f^2 > 0$, a version of the Central Limit Theorem for geometrically ergodic Markov chains [8] applies, so

$$T^{-1/2} \left(\sum_{k=0}^T f(X_k) - \mu f \right) \xrightarrow{D} N(0, \sigma_f^2),$$

with $\mu f = \int f(x)\mu(dx)$ for a probability measure μ and a μ -measurable function f . The effective sample size T_e is usually defined as

$$T_e = \frac{\text{Var}_{\mu}(f)T}{\sigma_f^2}, \quad (5)$$

²The actual implementation is slightly more complicated, and relies on `log1p` and `expm1` when mr is close to machine precision.

³Double precision machine ϵ is approximately 2.22×10^{-16} .

an adjustment to the path length T to reflect how much the asymptotic variance, σ_f^2 , is inflated by autocorrelation. To estimate T_e from paths of length T , we employ the procedure in `coda`, which uses an estimate of the spectral density at frequency zero.

Comparing estimates of T_e to the path length T quantifies the effect of autocorrelation on the efficiency of the algorithm, but it is not adequate by itself for comparing algorithms, since an algorithm with higher autocorrelations that requires less computation per step may still be more efficient than an algorithm with lower autocorrelations that requires more computation per step. Thus, we also compute T_e/t , effective samples per second of compute time t .⁴ Smaller T_e/t is an unambiguous criteria for superior efficiency, since the measure incorporates both the effect of autocorrelations and computation per step.

For reversible Markov operators, a well-known result – [6, Thm 2.1], see also [10] – relates the asymptotic variance to the $L^2(\mu)$ spectral gap $\delta(P)$ of the Markov operator P

$$\frac{\sigma_f^2}{\text{Var}_\mu(f)} \leq \frac{2}{\delta(P)} - 1. \quad (6)$$

This bound is sharp for worst-case functions when P has no residual spectrum, which holds, for example, for a reversible Markov kernel on a finite state space. Thus, a crude way of estimating how δ varies with n and p is to compute an estimate of T_e for different values of n and p , then approximate δ by T_e^{-1} via the upper bound in (6) combined with (5); because we take the logarithm, constants are irrelevant. Specifically, suppose $\delta = Bn^k p^j$, so $\log(\delta) = \log(B) + k \log(n) + j \log(p)$. Then one can obtain a rough estimate of the order of δ in p and n from a regression of $\log(T_e^{-1})$ on $\log(n)$ and $\log(p)$. Comparing estimates \hat{k}, \hat{j} of k, j across different algorithms is one way to empirically evaluate the relative computational complexity of the algorithms. Note that the spectral gap also gives finite-time error bounds [18].

4 Simulations

In this section we perform simulation studies varying n and p to compare our algorithm to that of Bhattacharya et al. [2], the most scalable algorithm proposed for this problem to date (that we are aware of).

4.1 Simulation setup

We vary n between 250 and 2,000 and p between 1,000 and 20,000. In each case, the true β , denoted $\beta^{(0)}$, is sparse, with

$$\begin{aligned} \beta_j^{(0)} &= 4, & j \leq 5 \\ \beta_j^{(0)} &= 2^{(6-j)/2}, & 6 \leq j \leq 15 \\ \beta_j^{(0)} &= 0, & j > 15 \end{aligned}$$

For each combination of n and p , we generate data as

$$\begin{aligned} x_{ij} &\sim N(0, 1), & 1 \leq j \leq p, 1 \leq i \leq n \\ y_i &\sim N(x_i \beta^{(0)}, 4). \end{aligned}$$

Simulations of this sort are quite standard in the literature on high-dimensional regression with sparse signals. To make the simulation more realistic, in addition to signals that are comparable to the noise variance, we also include a decreasing sequence of signals, many of which are small relative to the noise variance.

⁴All computations were performed using identical hardware in the same computing environment.

4.2 Results

Table 1 shows effective samples per second for ξ for our algorithm (“block”) compared to the algorithm of Bhattacharya et al. [2], which uses slice sampling to update ξ (designated “slice” in the figures and tables that follow). The efficiency ratio of the two algorithms is the ratio of T_e/t for the algorithm that uses the block update to the algorithm that uses slice sampling. For $p = 1,000$, our algorithm is between 4 and 7 times more efficient than the algorithm of Bhattacharya et al. [2], but for values of $p \geq 5,000$, our algorithm is between about 36 and 99 times more efficient than the algorithm of Bhattacharya et al. [2], with the relative efficiency of our algorithm increasing as p increases.

Table 1: Effective samples per second for ξ .

n	p	block	slice	efficiency ratio
500	1000	2.1772	0.2538	8.58
500	5000	0.6551	0.0182	36.05
500	10000	0.2581	0.0035	74.37
500	20000	0.0750	0.0009	87.98
1000	1000	0.5716	0.1191	4.80
1000	5000	0.2075	0.0051	40.37
1000	10000	0.0840	0.0017	49.00
1000	20000	0.0441	0.0004	98.68

Figure 1 shows a trace plot for ξ from both algorithms for $n = 1,000$ and $p = 20,000$. The high autocorrelation and small typical step sizes of the slice sampling update are evident. This results in the slice sampling algorithm badly underestimating the tails of the posterior for ξ .

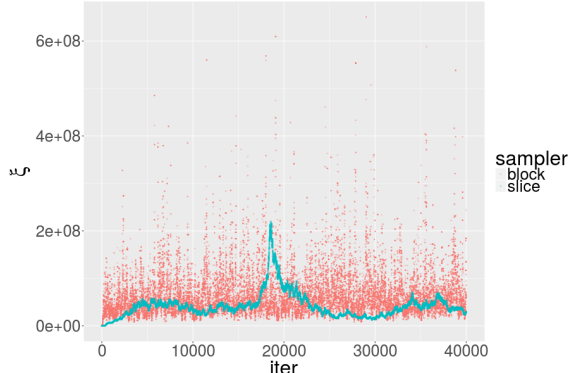


Figure 1: Trace plot for $n = 1000, p = 20,000$ for slice sampler (blue) and block update (red).

Figure 2 shows that improved mixing for ξ in our algorithm does not come at the expense of sampling efficiency for other parameters. The distribution of T_e/t for the first fifty entries of β and η — which includes the 15 components of β for which $\beta_j^{(0)} \neq 0$, as well as 35 entries for which $\beta_j^{(0)} = 0$ — is very similar for the two algorithms across the four values of p considered.

5 Analysis and implications

We now provide a more in-depth analysis of why constructing an efficient algorithm to sample ξ is challenging, and why our approach gives better results. We also provide empirical estimates of the computational complexity of our algorithm and the algorithm of Bhattacharya et al. [2].

Figure 3 shows a density estimate of the posterior for ξ and $\log(\xi)$ using our sampler and the slice sampling update of Bhattacharya et al. [2] for $p = 20,000$. The density estimate obtained using the path from the slice sampler is shifted toward zero relative to the density estimate obtained

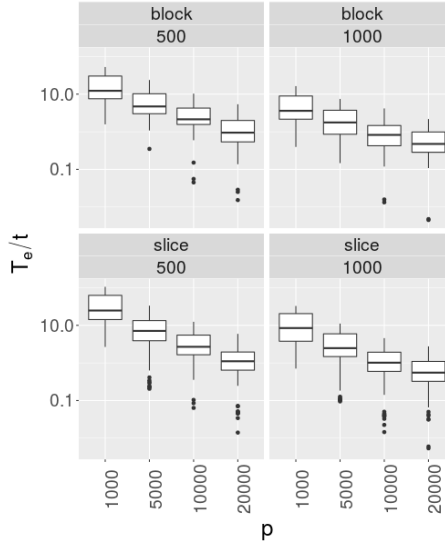


Figure 2: Boxplot of effective samples per second for the first fifty entries $\beta, \eta, n = 1,000$, varying p . The vertical axis is in a \log_{10} scale.

with the block MCMC sampler. The slice sampler apparently does a very poor job of exploring the tails of the posterior for ξ .

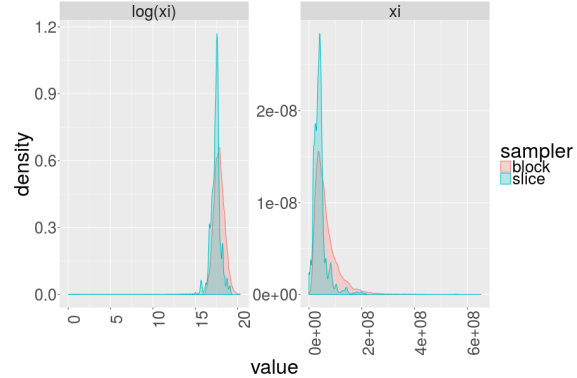


Figure 3: Density estimate for ξ and $\log(\xi)$ from MCMC paths for slice sampling algorithm and our block update with $n = 1000, p = 20,000$.

We estimated the tail index of the posterior for ξ using the sample path from the block update. Applying the Hill estimator using the 500 largest observations, we obtain an estimate of 0.25, suggesting that the posterior is very heavy tailed (this estimate was quite insensitive to the number of order statistics used in the estimation). This suggests an intuitive explanation for the good performance of the random walk proposal on $\log(\xi)$ used in our Metropolis-Hastings update: the posterior for ξ is evidently highly left-skewed, and as the proposal on the original (ξ) scale is lognormal, its variance is proportional to $\exp(2\xi_t)$. Therefore, the step sizes of the algorithm increase with the current state of ξ . When the state ξ_t is in the tail, large moves are proposed, allowing the algorithm to rapidly transition between the tails and the mode. In contrast, the slice sampler step sizes are insensitive to the current state, resulting in slow exploration of the target and slow transitions between the tails and the mode.

We approximate the computational complexity of the algorithm by estimating the order of growth in T_e^{-1} as a function of p . Recall from (6) that one can roughly approximate the rate at which the spectral gap converges to 1 by estimating the coefficients j, k in the model

$$\log(T_e^{-1}) = C + k \log n + j \log p. \quad (7)$$

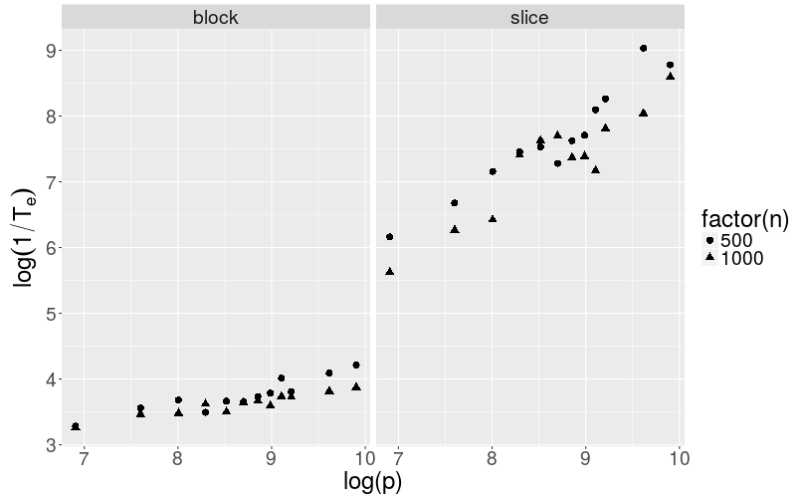


Figure 4: Plots of $\log(p)$ vs $-\log(T_e)$ for the slice sampler and block update for different values of n .

We estimated T_e for $p = 10^3, 2 \times 2^3, \dots, 10^4, 1.5 \times 10^4, 2 \times 10^4$ and $n = 500, 10^3$ using paths of length $T = 40,000$ in each case for both the block update and slice samplers. We then estimate a linear model of the form (7). For the slice sampling algorithm the estimate of j is -0.52 , while for the block update it is about -0.19 , indicating that larger n actually improves mixing. For the slice sampling algorithm, the point estimate of j was 0.91 , while for the block update, it was 0.24 . Plots of $\log(p)$ vs $\log(T_e^{-1})$ are shown in Figure 4. This implies that the overall computational complexity for the slice sampling algorithm is $\mathcal{O}(n^{1.5}p^{1.91})$, while for the block update it is approximately $\mathcal{O}(n^{1.8}p^{1.24})$. Thus, it is possible that the slice sampler might be superior for large n , small p cases. However, these priors are designed for large p , small n , justifying our focus on this setting. Why larger n improves mixing is not entirely clear, though it seems likely to be related to the phenomenon we now describe, as growing n with fixed signal size will tend to result in few signals near the threshold of detection.

Finally, we show some empirical evidence that suggests further improvement in performance of the algorithm may be possible. In both the block and slice sampling algorithms, when the true value of β_j is small but nonzero, the posterior appears to be bimodal, with one mode very near zero, and another near the true value of β_j . This is evident in the trace plot for β_{10} (recall $\beta_{10}^{(0)} = 0.25$) in Figure 5. Another obvious feature of this trace plot is that both Markov chains are slow to transition between the two modes, remaining in one or another neighborhood for many iterations before transitioning back. It is exactly a few components of β that are small but nonzero that result in the outliers in Figure 5. We conjecture that when $\beta_j^{(0)}$ is near the minimax-optimal adaptive threshold, the posterior will be bimodal, and slow transitions between the two modes can arise. One way to improve mixing for these components of β would be to use Metropolis-Hastings to sample these few components of β conditional on all of the others. To make this approach tractable, one could perform an initial thresholding or empirical Bayes procedure to identify signals that are likely to be near the threshold of detection.

6 Discussion

Despite the popularity of scale-mixture priors, and in particular global-local family priors, in high-dimensional Bayesian statistics, efficient computational algorithms for these models have been elusive. Gibbs sampling algorithms for these models date at least to [13]. The hybrid Gibbs-slice sampling algorithms of Polson et al. [15] were further developed by Bhattacharya et al. [2], which considerably reduced the computational cost per step of these algorithms, but did not address slow mixing of the global scale. Here we construct a block update for β, σ^2, ξ that achieves significantly improved computational efficiency for ξ , and show that the computational complexity resulting from autocorrelation for our algorithm is a small fractional power of p . In other words,

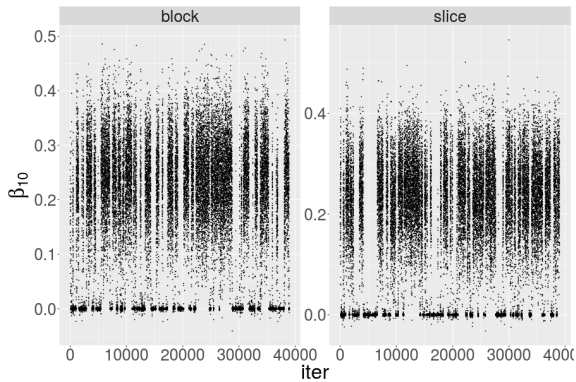


Figure 5: Trace plot for β_{10} for $n = 1000, p = 20,000$.

the convergence rate of the algorithm is only weakly dependent on dimension.

Algorithms for this particular class of Bayesian model have been under active development for almost a decade, and only through the combined efforts of several groups is it now possible to scale computation to tens of thousands of predictors. It is arguably revealing that the major improvements in computational efficiency have not resulted from applying exotic computational methods, but rather from a clever use of known linear algebraic identities and application of two common tools for improving MCMC performance: block updating and judicious choice of a proposal distribution for a Metropolis-Hastings update. It seems likely that further progress in scaling computation for other common Bayesian methods for high-dimensional problems may result from similar application of a combination of known tools.

A Additional results

Table 2 shows effective samples per second for σ^2 for the block update and slice sampling algorithms. For larger values of p , the relative efficiency of our algorithm for σ^2 is very similar, and is never less than about 0.5.

Table 2: Effective sample size per second for σ^2

n	p	block	slice
500	1000	3.779	7.850
500	5000	0.552	0.733
500	10000	0.146	0.168
500	20000	0.038	0.042
1000	1000	2.566	5.667
1000	5000	0.327	0.503
1000	10000	0.089	0.108
1000	20000	0.033	0.038

Figure 6 provides another validation of the performance of our algorithm with respect to sampling ξ . Autocorrelations at lags 1-100 are considerably lower for our algorithm than the algorithm of Bhattacharya et al. [2], indicating superior efficiency.

Figure 7 shows the distribution of estimated lag- k autocorrelations for $k = 1, 5, 10, \dots, 100$ for the block update compared to the slice sampling algorithm. The results are again very similar between the two algorithms across the different values of p considered. This provides further evidence that improved efficiency for sampling ξ in our algorithm does not come at the expense of efficiency for sampling other parameters.

Figure 8 shows a trace plot for $\log(\xi)$ produced by the algorithm of Bhattacharya et al. [2] without removing the numeric truncations used in the code. This plot was produced with $n = 500, p = 10,000$, and $T = 40,000$ iterations. It is clear that convergence has not yet occurred. This

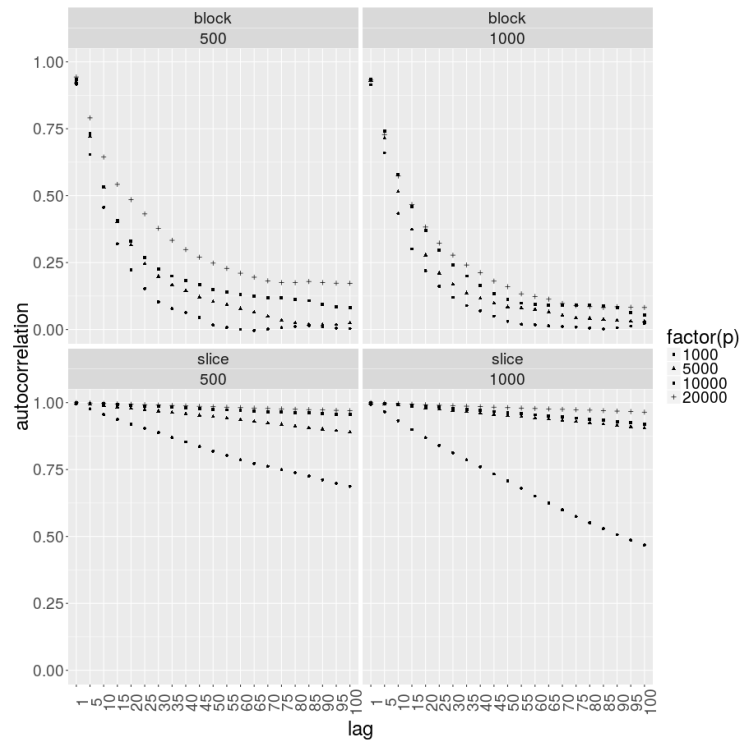


Figure 6: Autocorrelation function for ξ for varying n and p for both samplers.

phenomenon did not occur in any of the simulations we ran using our method for slice sampling of η (compare to Figure 1, which shows a trace plot for ξ for our algorithm in pink), which obviates the need for numeric truncations.

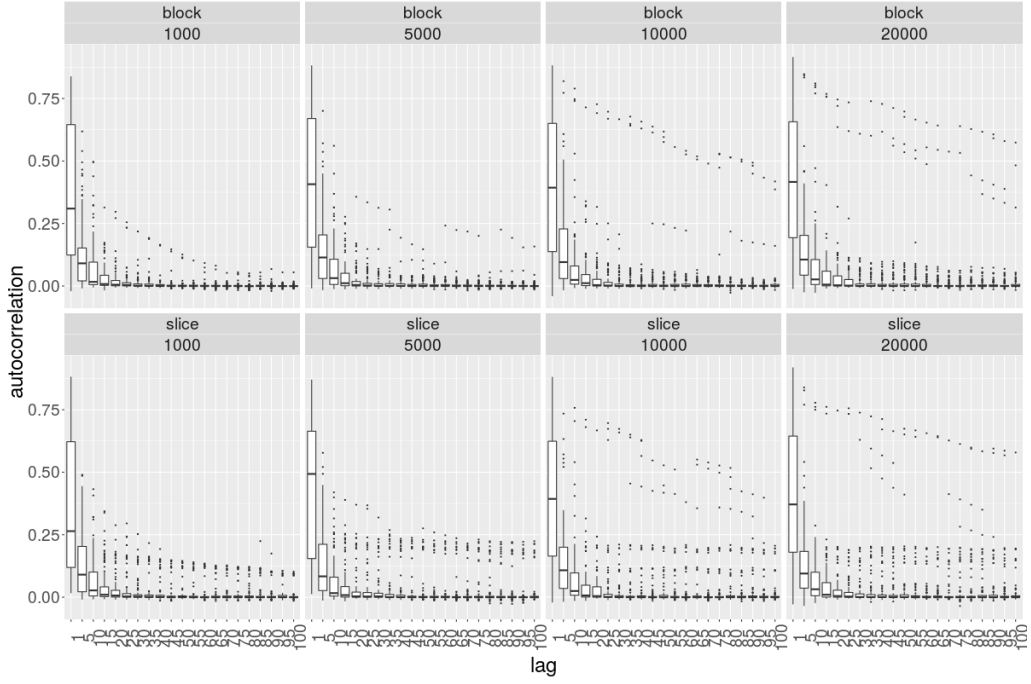


Figure 7: Boxplot of autocorrelation function for the first fifty entries β, η , $n = 1,000$, varying p .

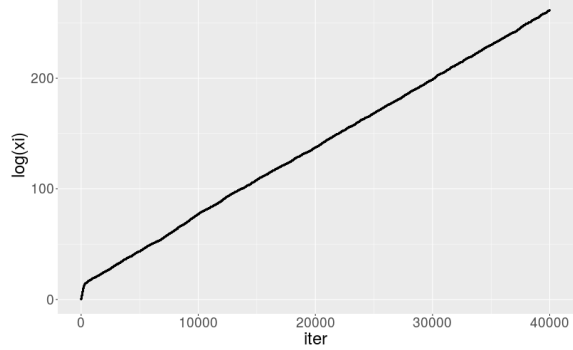


Figure 8: Trace plot for $\log(\xi)$ using the algorithm of Bhattacharya et al. [2] exactly as provided in the code.

B Derivation of MCMC algorithm

B.1 Update for $p(\xi | \eta, y)$

To find the update for $p(\xi | \eta, y)$, first note that

$$\begin{aligned}
 p(\tau | \lambda, y) &= \int p(\tau, \sigma^2 | \lambda, y) d\sigma^2 \propto \int p(y | \lambda, \tau, \sigma^2) p(\tau | \lambda, \sigma^2) p(\sigma^2) d\sigma^2 \\
 &\propto p(\tau) \int p(y | \lambda, \tau, \sigma^2) (\sigma^2)^{-a_0/2-1} e^{-b_0/(2\sigma^2)} d\sigma^2 \\
 &= \frac{1}{1 + \tau^2} \int N(0, \sigma^2 (X(\text{diag}(\tau\lambda))^2 X^T + I)) (\sigma^2)^{-a_0/2-1} e^{-b_0/(2\sigma^2)} d\sigma^2 \\
 &= \frac{1}{1 + \tau^2} |X(\text{diag}(\tau\lambda))^2 X^T + I|^{-1/2} \int (\sigma^2)^{-n/2-a_0/2-1} e^{-\frac{1}{s\sigma^2}[(y^T (X(\text{diag}(\tau\lambda))^2 + I)^{-1} y) + b_0]} d\sigma^2,
 \end{aligned}$$

so computing the integral and changing variables $\tau \mapsto \xi$, we obtain

$$p(\tau \mid \lambda, y) \propto \frac{1}{1 + \tau^2} \frac{1}{|X(\text{diag}(\tau\lambda))^2 X^T + I|^{1/2}} (y^T (X(\text{diag}(\tau\lambda))^2 X^T + I)^{-1} y + b_0)^{-(n+a_0)/2} \\ \propto \xi^{-3/2} \frac{\xi}{\xi + 1} \frac{1}{|X\xi^{-1}(\text{diag}(\lambda))^2 X^T + I|^{1/2}} (y^T (X\xi^{-1}(\text{diag}(\lambda))^2 X^T + I)^{-1} y + b_0)^{-(n+a_0)/2}.$$

Now, changing variables $\lambda \mapsto \eta$, we get

$$p(\xi \mid \eta, y) \propto \frac{1}{\sqrt{\xi}(1 + \xi)} \frac{1}{|X\xi^{-1}\text{diag}(\eta^{-1})X^T + I|^{1/2}} (y^T (\xi^{-1} X \text{diag}(\eta^{-1}) X^T + I)^{-1} y + b_0)^{-\frac{n+a_0}{2}},$$

where $\text{diag}(\eta^{-1})$ refers to the diagonal matrix with elements η_j^{-1} .

B.2 Update for $p(\sigma^2 \mid \xi, \eta, y)$

Since $p(\sigma^2 \mid \tau, \lambda, y) \propto p(y \mid \tau, \lambda, \sigma^2) p(\sigma^2)$, let us consider $p(y \mid \tau, \lambda, \sigma^2)$. We can rewrite our model as

$$\begin{aligned} \beta &= \varepsilon_1, & \varepsilon_1 &\sim N(0, \sigma^2 \tau^2 \text{diag}(\lambda_1^2, \dots, \lambda_p^2)) \\ y &= X\beta + \varepsilon_2, & \varepsilon_2 &\sim N(0, \sigma^2 I), \end{aligned}$$

so

$$y = X\varepsilon_1 + \varepsilon_2 \sim N(0, \sigma^2 (X(\text{diag}(\tau^2 \lambda_1^2, \dots, \tau^2 \lambda_p^2)) X^T + I)).$$

Thus,

$$p(\sigma^2 \mid \xi, \eta, y) \propto \frac{1}{(\sigma^2)^{n/2}} e^{-\frac{1}{2\sigma^2} (y^T (X \text{diag}((\xi\eta_1)^{-1}, \dots, (\xi\eta_p)^{-1}) X^T + I)^{-1} y)} \frac{1}{(\sigma^2)^{a_0/2+1}} e^{-b_0/(2\sigma^2)} \\ \propto \text{InvGamma} \left(\frac{n+a_0}{2}, \frac{1}{2} [y^T (X(\text{diag}(\xi\eta))^{-1} X^T + I)^{-1} y + b_0] \right)$$

B.3 Update for $p(\beta \mid \sigma^2, \xi, \eta, y)$

Since the $p(\beta \mid \sigma^2, \tau, \lambda, y)$ is proportional to

$$\begin{aligned} p(\beta \mid \sigma^2, \tau, \lambda, y) &= p(y \mid \beta, \sigma^2, \tau, \lambda) p(\beta \mid \tau, \lambda, \sigma^2) \\ &\propto e^{-\frac{1}{2\sigma^2} (y - X\beta)^T (y - X\beta)} \prod_{j=1}^p e^{-\frac{1}{2\sigma^2 \tau^2 \lambda_j^2} \beta_j^2} \\ &= e^{-\frac{1}{2\sigma^2 \tau^2} (y - X\beta)^T (y - X\beta) - \frac{1}{2\sigma^2 \tau^2} \beta^T (\text{diag}(\lambda^2))^{-1} \beta}, \end{aligned}$$

changing the parameters $\tau \mapsto \xi$ and $\lambda \mapsto \eta$, and completing the square, we see that

$$\begin{aligned} p(\beta \mid \sigma^2, \xi, \eta, y) &\propto \exp \left(-\frac{1}{2\sigma^2} [y^T y - 2y^T X\beta + \beta^T X^T X\beta + \beta^T (\text{diag}(\xi\eta))\beta] \right) \\ &\propto \exp \left(-\frac{1}{2\sigma^2} [\beta^T (X^T X + \text{diag}(\xi\eta))\beta - 2y^T X\beta] \right) \\ &\sim N \left((X^T X + \text{diag}(\xi\eta))^{-1} X^T y, \sigma^2 (X^T X + \text{diag}(\xi\eta))^{-1} \right). \end{aligned}$$

B.4 Update for $p(\eta \mid \beta, \sigma^2, \xi, y)$

We start by writing

$$\begin{aligned} p(\lambda \mid \beta, \sigma^2, \tau, y) &\propto p(y \mid \beta, \lambda, \tau, \sigma^2) p(\beta \mid \lambda, \tau, \sigma^2) p(\lambda) = p(\beta \mid \lambda, \tau, \sigma^2) p(\lambda) \\ &= \prod_{j=1}^p p(\beta_j \mid \lambda_j, \tau, \sigma^2) p(\lambda_j), \end{aligned}$$

so we can decompose the problem into the update for each λ_j . Then, the change of variables $\lambda_j \mapsto \eta_j$ gives

$$\begin{aligned} p(\beta_j \mid \lambda_j, \tau, \sigma^2) p(\lambda_j) &= \frac{1}{\sqrt{2\pi\sigma^2\tau^2\lambda_j^2}} e^{-\frac{1}{2\sigma^2\tau^2\lambda_j^2}\beta_j^2} \frac{1}{1+\lambda_j^2} \\ &\propto \eta_j^{1/2} \frac{\eta_j}{\eta_j + 1} e^{-\frac{\xi\eta_j}{2\sigma^2}\beta_j^2} \eta_j^{-3/2} \\ &= \frac{1}{\eta_j + 1} e^{-\frac{\xi\beta_j^2}{2\sigma^2}\eta_j}. \end{aligned}$$

We sample from this density by performing slice sampling. For each j , we first sample a truncated uniform U , and then sample η_j conditional on $U = u$ according to:

1. $U \mid \eta_j \sim \text{Unif}\left[0, \frac{1}{1+\eta_j}\right]$;
2. $\eta_j \mid u \sim e^{-\frac{\xi\beta_j^2}{2\sigma^2}\eta_j} \mathbb{I}_{[\frac{1-u}{u} > \eta_j]}$.

References

- [1] Armagan, A., Dunson, D. B., and Lee, J. (2013). Generalized double Pareto shrinkage. *Statistica Sinica*, 23(1):119.
- [2] Bhattacharya, A., Chakraborty, A., and Mallick, B. K. (2016). Fast sampling with Gaussian scale mixture priors in high-dimensional regression. *Biometrika*, page asw042.
- [3] Bhattacharya, A., Pati, D., Pillai, N. S., and Dunson, D. B. (2015). Dirichlet–Laplace priors for optimal shrinkage. *Journal of the American Statistical Association*, 110(512):1479–1490.
- [4] Diaconis, P., Khare, K., and Saloff-Coste, L. (2008). Gibbs sampling, exponential families and orthogonal polynomials. *Statistical Science*, 23(2):151–178.
- [5] George, E. I. and McCulloch, R. E. (1997). Approaches for Bayesian variable selection. *Statistica sinica*, pages 339–373.
- [6] Geyer, Charles J (1992). Practical Markov chain Monte Carlo. *Statistical Science*, pages 473–483.
- [7] Hans, C. (2009). Bayesian lasso regression. *Biometrika*, pages 835–845.
- [8] Jones, G. L. (2004). On the Markov chain central limit theorem. *Probability surveys*, 1(299–320):5–1.
- [9] Khare, K. and Hobert, J. P. (2013). Geometric ergodicity of the Bayesian lasso. *Electronic Journal of Statistics*, 7:2150–2163.
- [10] Kipnis, C. and Varadhan, S. S. (1986). Central limit theorem for additive functionals of reversible Markov processes and applications to simple exclusions. *Communications in Mathematical Physics*, 104(1):1–19.
- [11] Makalic, E. and Schmidt, D. F. (2016). A simple sampler for the horseshoe estimator. *IEEE Signal Processing Letters*, 23(1):179–182.
- [12] Pal, S. and Khare, K. (2014). Geometric ergodicity for Bayesian shrinkage models. *Electronic Journal of Statistics*, 8(1):604–645.
- [13] Park, T. and Casella, G. (2008). The Bayesian lasso. *Journal of the American Statistical Association*, 103(482):681–686.

- [14] Polson, N. G. and Scott, J. G. (2010). Shrink globally, act locally: Sparse Bayesian regularization and prediction. *Bayesian Statistics*, 9:501–538.
- [15] Polson, N. G., Scott, J. G., and Windle, J. (2014). The Bayesian bridge. *Journal of the Royal Statistical Society: Series B (Statistical Methodology)*, 76(4):713–733.
- [16] Rajaratnam, B. and Sparks, D. (2015). MCMC-based inference in the era of big data: A fundamental analysis of the convergence complexity of high-dimensional chains. *arXiv preprint arXiv:1508.00947*.
- [17] Rajaratnam, B., Sparks, D., Khare, K., and Zhang, L. (2017). Scalable Bayesian shrinkage and uncertainty quantification in high-dimensional regression. *arXiv preprint arXiv:1703.09163*.
- [18] Rudolf, D. (2011). Explicit error bounds for Markov chain Monte Carlo. *arXiv preprint arXiv:1108.3201*.
- [19] Scott, J. G. and Berger, J. O. (2010). Bayes and empirical-Bayes multiplicity adjustment in the variable-selection problem. *The Annals of Statistics*, 38(5):2587–2619.
- [20] Smith, A. F. and Roberts, G. O. (1993). Bayesian computation via the Gibbs sampler and related Markov chain Monte Carlo methods. *Journal of the Royal Statistical Society. Series B (Methodological)*, pages 3–23.
- [21] Strawderman, W. E. (1971). Proper Bayes minimax estimators of the multivariate normal mean. *The Annals of Mathematical Statistics*, 42(1):385–388.
- [22] Tibshirani, R. (1996). Regression shrinkage and selection via the lasso. *Journal of the Royal Statistical Society. Series B (Methodological)*, pages 267–288.
- [23] Van Der Pas, S., Kleijn, B., and Van Der Vaart, A. (2014). The horseshoe estimator: Posterior concentration around nearly black vectors. *Electronic Journal of Statistics*, 8(2):2585–2618.